# Electronic Supplementary Information

# Anti-pressure, fatigue resistance and rapid self-healing hydrogel based on nano-micelle assembly

Zhiang Shao,[a] Weimin Cheng, [a] Xiangming Hu,*[,a,b] Yanyun Zhao,[c] Peng Wang,[c] Mingyue Wu,[a] Di Xue,[a] Jiaoyun Hou,[a] and Susu Bian[a]

[a]College of Mining and Safety Engineering, Shandong University of Science and Technology Qingdao, Shandong 266590, China

[b]College of Resources and Environmental Engineering, Binzhou University Binzhou, Shandong 256603, China

[c]College of Chemical and Environmental Engineering, Shandong University of Science and Technology Qingdao, Shandong 266590, China

* Corresponding authors.

E-mail addresses: xiangming0727@163.com

## Materials

Methacryloyloxyethyltrimethylammonium chloride (DMC, Aladdin, 75% in the water), 4-styrenesulfonic acid sodium salt (NaSS, Aladdin, 90%), anhydrous acetic acid (Aladdin, 99.0%), acrylamide (AM, Aladdin, 99.0%), N,N'-methylenebisacrylamide (MBA, Aladdin, 99.0%), ammonium persulfate (APS, Aladdin, 98%), N,N,N',N'-tetramethylethylenediamine (TEMED, Aladdin, 99.0%). All chemicals were used as received without further purification.

## Synthesis of methacryloyloxyethyltrimethylammonium chloride/(4-styrenesulfonic acid) sodium dimer (DMC-NaSS) and hydrogel

**Synthesis of methacryloyloxyethyltrimethylammonium chloride/(4-styrenesulfonic acid) sodium dimer (DMC-NaSS).** The three-necked round bottomed flask was purged with nitrogen gas three times before use. First, deionized water (30 mL) was injected to the three-necked flask, then 8.31 g DMC (1 M) and 6.99 g NaSS (1 M) were sequentially added. The mixture was magnetically stirred at 35 °C for 10 min under a nitrogen atmosphere. Finally, anhydrous acetic acid (120 μL) of was added to the homogeneous system and reaction heated to 50 °C with stirring. After 40 min, a DMC-NaSS solution was obtained.

**Synthesis of the hydrogel.** The temperature of the obtained DMC-NaSS solution was lowered to 35 °C. AM (3.0 g) was added and the mixture stirred for an additional 30 min with a magnetic stirrer until AM was sufficiently dissolved.Crosslinker N,N-methylenebisacrylamide (12.8 mg) and catalyst TEMED (90 μL) were added to the reaction system and allowed to stir with a magnetic stirrer at 35 °C for an additional 30 min. Pre-prepared initiator ammonium persulfate solution (450 μL, 0.4 g of ammonium persulfate in 5 mL deionized water) was transferred to the reaction system and stirred

for 10 min to obtain a uniform solution. Finally, the fully mixed solution was transferred to 15 mL sampling bottles (3 bottles), which were then placed in a thermostatic water bath at 60 °C for 24 h producing a transparent hydrogel with a light blue color. We further studied the effect of DMC-NaSS concentration on the gel's properties, and found that the presence of DMC-NaSS in the system requires excess APS for the gelation reaction. Reasons for this necessity include a greater amount of reactive monomer will consume APS[1] or the occurrence of self-polymerization between DMC-NaSS. More importantly, the gel has a definite concentration range for the gelation reaction to proceed, namely, hydrogel formation only occurs between 0.5-1.5 M DMC-NaSS concentration (Figure S1). When the concentration of DMC-NaSS is too low (<0.5 M), the stability of the micelles is poor and dispersed, which can't form an effective crosslinked structure. In fact, the gelation process of DMC-NaSS gel is accompanied by two forms, one is the polymerization process of the reactive monomer; the other is the phase separation process of the hydrophilic phase and the hydrophobic phase in the system. The phase separation process of the gel can be expressed by the Flory-Huggins equation.

$$\Delta G = RT\left[\left(\phi_1 / P_1\right)\ln\phi_1 + \left(\phi_2 / P_2\right)\ln\phi_2 + \chi^{12}\phi_1\phi_2\right] \quad (1\text{-}1)$$

Among them: Φ and P are the volume fraction and the polymerization degree of one component in the system, respectively. Subscript 1 and 2 are respectively 2 different components; $\chi^{12}$ is the interaction parameter of the two components. The first two items on the right side of the equation are entropy variables, and the last one is the metamorphosis item. As the degree of polymerization of "1" or "2" phases increases, the degree of freedom of chemical coordination decreases, resulting in a decrease in the

absolute value of entropy change, a change in free energy from negative to positive, and the original uniform system becomes unstable. Phase separation begins to appear. When the concentration of DMC-NaSS is between 0.5 and 1.5 M, the micelle size will increase during the polymerization process (Fig. S1c), indicating that the polymerization process coincides with the phase separation process. The hydrophilic phase and the hydrophobic phase form a three-dimensional connected structure on the sodium scale to obtain a blue transparent gel (Fig. S1b). However, when the concentration of DMC-NaSS is too high (>1.5M), the hydrophilicity of the solvent phase and the hydrophobic phase are too large, resulting in an increase in the polymerization degree of the hydrophobic phase, and the phase separation becomes very significant. The hydrophobic phase breaks into spherical particles (the spherical surface has the smallest surface area and the lowest surface energy) and are separated from the aqueous phase (Fig. S1a).

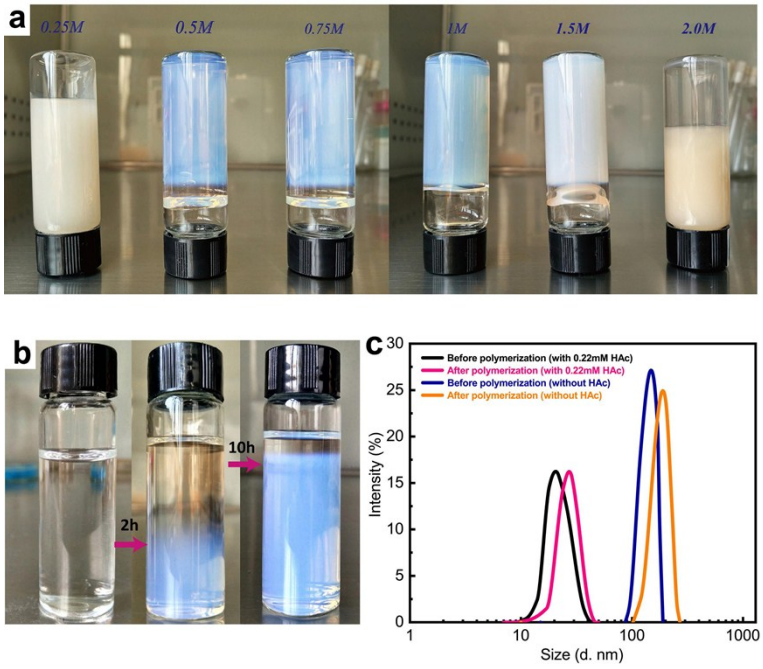


**Figure S1.** (a) Suitable DMC-NaSS contents (0.5M~1.5M) resulted in solid hydrogels. Low contents ($C_{DMC\text{-}NaSS}$＜0.5M） or higher contents ($C_{DMC\text{-}NaSS}$＞1.5M) resulted in

viscous solution. (b) Pictures of polymerization solutions at different instants of time. (c) Size distributions of DMC-NaSS micelles in the solution of different reaction time.

**Table 1.** DMC-NaSS solution composition table for DLS, TEM, and rheology experiments.

| code | HAc (μl) | DMC (g) | NaSS (g) | Water (ml) |
|---|---|---|---|---|
| HAc - 0mM | 30 | 8.31 | 6.99 | 30 |
| HAc - 0.055mM | 60 | 8.31 | 6.99 | 30 |
| HAc - 0.11mM | 120 | 8.31 | 6.99 | 30 |
| HAc - 0.22mM | 240 | 8.31 | 6.99 | 30 |
| HAc - 0.44mM | 480 | 8.31 | 6.99 | 30 |

**Table 2.** DMC-NaSS gel composition table for TEM and mechanical property experiments.

| code | HAc (mM/) | HAc (μL) | DMC (g) | NaSS (g) | AM (g) | APS (mg) | TMEDE (μL) | MBA (mg) | Water (mL) |
|---|---|---|---|---|---|---|---|---|---|
| 0.5M | 0.22 | 120 | 4.155 | 3.495 | 3.0 | 36 | 90 | 12.8 | 30 |
| 0.75M | 0.22 | 120 | 6.233 | 5.243 | 3.0 | 36 | 90 | 12.8 | 30 |
| 1M | 0.22 | 120 | 8.31 | 6.99 | 3.0 | 36 | 90 | 12.8 | 30 |
| PAM | 0 | 0 | 0 | 0 | 9 | 36 | 90 | 12.8 | 30 |

## FT-IR analysis

**Experimental:** In order to explore the weak interactions existing between PDMC and PNaSS, the effect of HAc on it's functional groups, as well as proving that there are no large Numbers of unreactive monomers (double bonds) in the gel, FT-IR analysis[3] of AM, PAM, PAM-PDMC, PAM-PNaSS, PAM-PDMC-PNaSS (DMC-NaSS gel without HAc) and PAM-PDMC-PNaSS/HAc (DMC-NaSS gel) was conducted. The experiment was conducted using FT-IR (Nicolet 5700, Germany) with a spectral width of 500-4000 $cm^{-1}$. Before measurement, the samples were freeze-dried for 48h.

**Results:** As shown in Figure S2, AM exhibits characteristic peaks at 3035.05, 1674 and 1604.72 $cm^{-1}$, corresponding to C-H stretching of -$CH{=}CH_2$, C=O stretching and C=C stretching, respectively. PAM have characteristic peaks at 2954 and 2855 $cm^{-1}$

, corresponding to C-H asymmetrical stretching and C-H symmetrical stretching of -$CH_2$-. PAM-PDMC exhibits characteristic peak at 2990 and 1397.65, corresponding to C-H stretching of -$CH_3$, C-N stretching of -$NC_3$, respectively. PAM-PNaSS have characteristic peaks at 1396.86 and 1039.95 $cm^{-1}$, corresponding to S=O asymmetrical stretching and S=O symmetric stretching, respectively.

**Analysis:** The characteristic peaks of double bonds (C-H stretching of -$CH{=}CH_2$, C=C stretching) disappear in the PAM-PDMC-PNaSS and the PAM-PDMC-PNaSS/HAc gels, suggesting that the polymerization reaction nearly consume all the unsaturated

monomer. The characteristic peak of quaternary ammonium (C-N stretching of -$NC_3$) appears at 1396.86 $cm^{-1}$ for PAM-PDMC-PNaSS, which showing a slight 0.79 $cm^{-1}$ red shift, compared with PAM-PDMC (1397.65 $cm^{-1}$). Similarly, PAM-PDMC-PNaSS shows the characteristic peaks of the sulfonic group at 1173.75 (asymmetric stretching vibrations of S=O), 1036.83 $cm^{-1}$ (symmetric stretching vibrations of S=O), which showing a 12.13 $cm^{-1}$ and 3.12 $cm^{-1}$ red shift, respectively, compared with PAM-PNaSS (1173.75 $cm^{-1}$ and 1106.83 $cm^{-1}$). Which confirms the electrostatic interaction between PDMC and PNaSS, that restrains the vibration of the C-N of quaternary ammonium and the S=O of sulfonic group. By comparing PAM-PDMC-PNaSS and PAM-PDMC-PNaSS/HAc, it can be seen that the characteristic peak of the sulfonic acid group has a red shift of 0.49, while the characteristic peak of the quaternary amine group has a blue shift of 0.14 and 0.09, indicating that the dipole moment interaction between the carboxyl group of HAc and quaternary ammonium will slightly weaken the electrostatic interaction between the quaternary amine group and the sulfonic acid group.

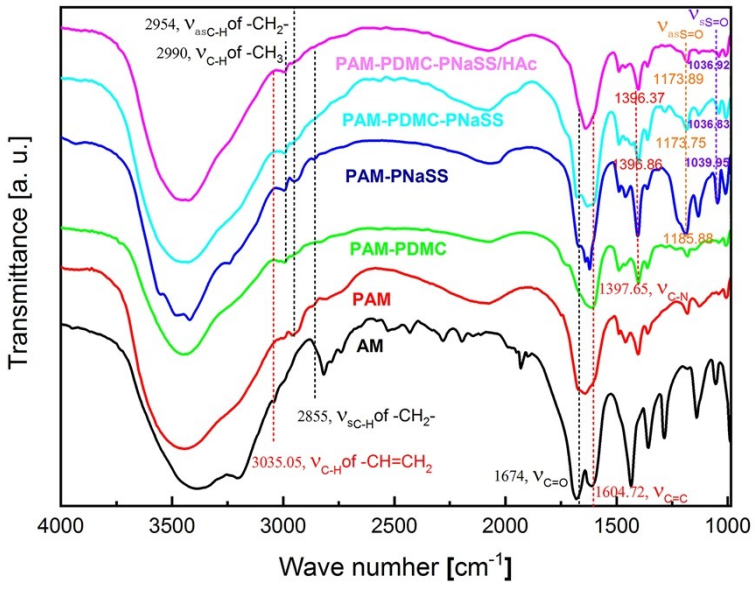


**Figure S2.** The FT-IR spectra of PAM-PDMC(1M AM/1M DMC), PAM-PNaSS (1.6M AM/0.4M NaSS) and PAM-PDMC-PNaSS (1M DMC-NaSS/1M AM) hydrogels.

## $^1$H NMR Analysis of polymer monomers

In order to investigate possible interactions between DMC and NaSS, $^1$H NMR analysis[4] was conducted for DMC, NaSS and DMC-NaSS. Deuterium oxide ($D_2O$) was used as the solvent and the samples were measured using a JEOL 600 spectrometer (600 MHz). DMC and NaSS $^1$H NMR spectra were measured in $D_2O$ and compared with the spectra standard listed in the biological NMR database. The signals of interest are the methyl protons of the nitrogen atoms (in the blue wireframe of Figure S3a, δ=3.61 ppm) and the aromatic protons adjacent the sulfonic group (in the red wireframe of Figure S3b, δ=7.83ppm).

Figure S3 shows the spectra of DMC, NaSS, and DMC-NaSS. **DMC** $^1$H NMR (600 MHz, $D_2O$) δ (ppm) 6.44-6.42 (m, 1H, C=$CH_2$), 6.06-6.05 (m, 1H, C=$CH_2$), 4.93-4.90 (m, 2H, -COO-$CH_2$), 4.20-4.17 (m, 2H, -$CH_2$-$NC_3$), 3.61 (s, 9H, -N($CH_3$)$_3$), 2.19 (s, 3H, -$CH_3$).

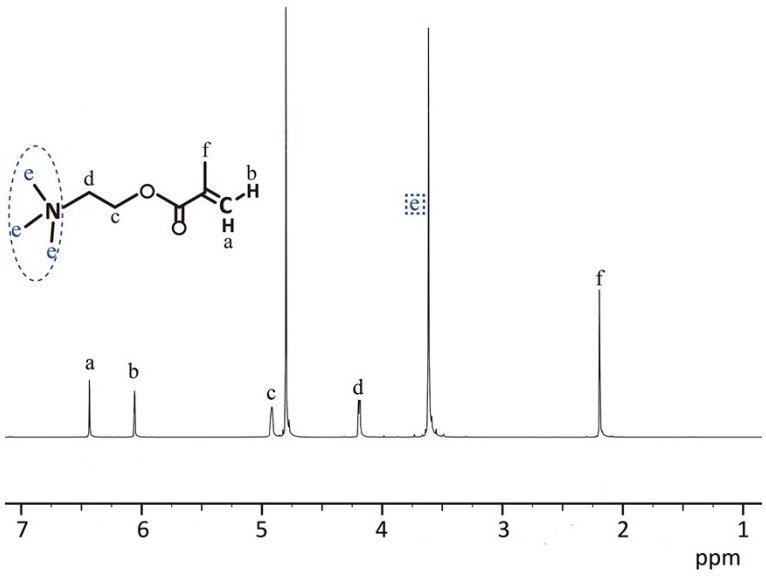


**Figure S3a.** The $^1$H NMR spectrum of DMC in $D_2O$.

**NaSS** $^1$H NMR (600 MHz, $D_2O$) δ (ppm) 7.83 (d, 2H, benzene ring hydrogen

adjacent to the sulfonic group), 7.51-7.40 (m, 2H, benzene ring hydrogen adjacent to the alkene), 6.64 (ddd, 1H, alkene hydrogen adjacent to the benzene ring), 5.80 (dd, 1H, $C=CH_2$), 5.33 (dd, 1H, $C=CH_2$).

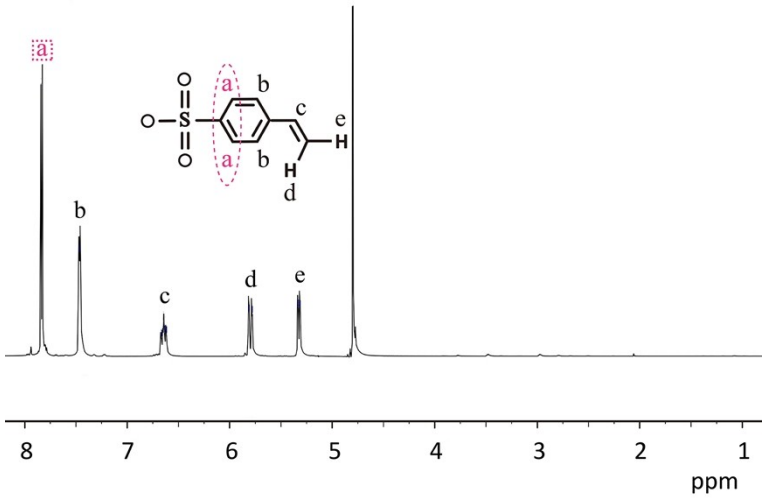


**Figure S3b.** The 1H NMR spectrum of NaSS in $D_2O$.

**DMC-NaSS** $^1H$ NMR (600 MHz, $D_2O$) δ (ppm) 7.79 (d, 2H, benzene ring hydrogen adjacent to sulfonic group), 7.64 (d, 2H, benzene ring hydrogel adjacent to alkene), 6.88 (s, 2H, alkene hydrogen adjacent to benzene ring), 6.17 (t, 1H, $C=CH_2$ in DMC), 6.01-5.95 (m, 1H, $C=CH_2$ in DMC), 5.82-5.75 (m, 1H, $C=CH_2$ in NaSS), 5.48-5.42 (m, 1H, $C=CH_2$ in NaSS), 3.80-3.77 (m, 2H, $-CH_2-NC_3$), 3.23 (s, 9H, $-N-(CH_3)_3$), 1.95 (s, 3H, $-CH_3$ in DMC).

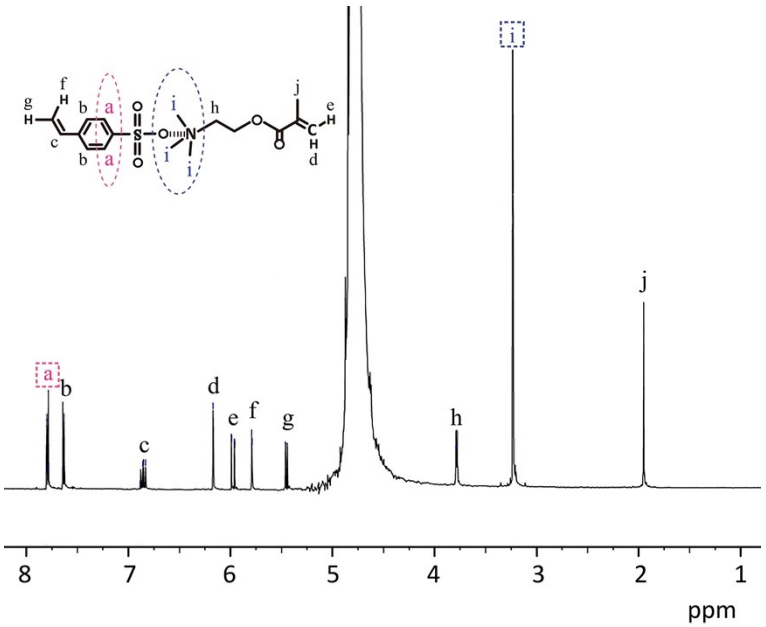


**Figure S3c.** The $^{1}H$ NMR spectrum of DMC-NaSS in $D_2O$.

Compared with the proton peaks of DMC quaternary ammonium (e(s) 3.61 ppm), DMC-NaSS shows a right shift of 0.58 ppm (i(s) 3.23 ppm) (Figure S10c). In the case of the aromatic protons adjacent the sulfonic group in NaSS (a(d) 7.83 ppm. DMC-NaSS shows a right shift of 0.04 ppm (a(d) 7.79ppm). This is because the electrostatic interaction between the quaternary ammonium group and the sulfonic acid group having a shielding effect on the hydrogen atom and causing the chemical shift value of the hydrogen atom.

## $^1$H NMR Analysis of DMC-NaSS Gel

**Preparation of DMC-NaSS gel.**

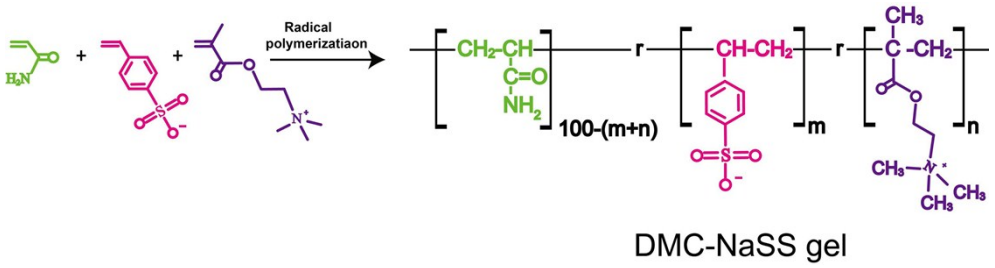


**Figure S4.** Preparation of DMC-NaSS gel

A DMC-NaSS gel was prepared by radical-copolymerization of acrylamide (1 mol), DMC (0.5 mol), NaSS (0.5 mol) and HAc (0.022 mmol) by a radial polymerization using ammonium peroxodisulfate (APS) (0.05 mol) and N,N,N',N'-tetramethylethane-1,2-diamine. (TEMED) (0.23 mol) in water at room temperature. In order to accurately characterize the distribution of the three reactive monomers on the polymer chain, the gel was dialyzed in deionized water for 48 h prior to testing.

**Characterization of DMC-NaSS gel.**

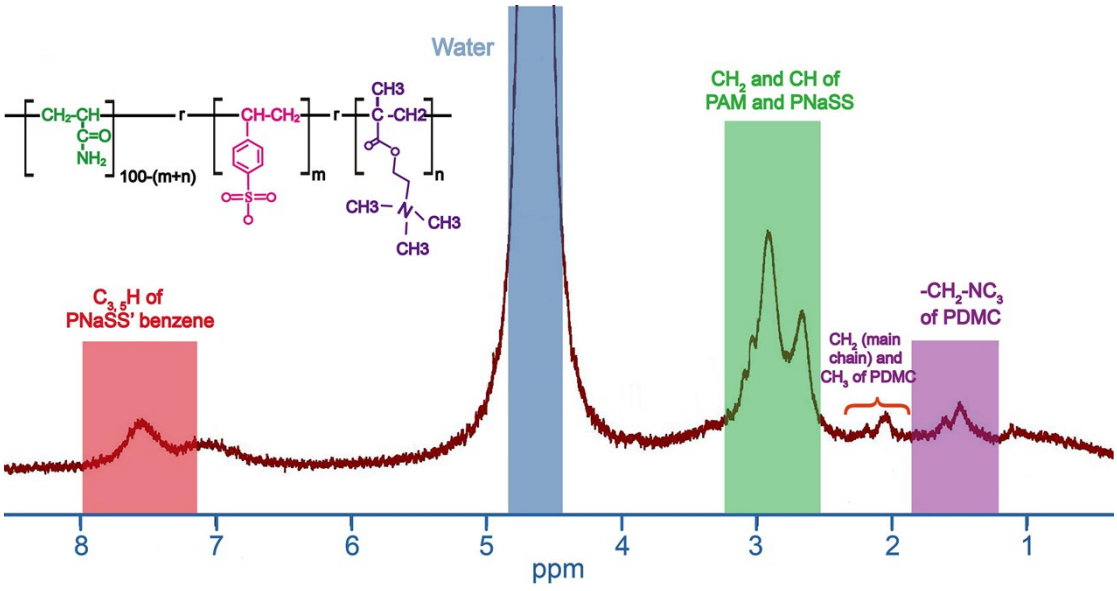

**Figure S5.** 400 MHz $^{1}H$ NMR spectra of DMC-NaSS gel in $D_2O$ at 30 ℃.

As shown in Figure S5, $C_{3,5}H$ of PNaSS'benzene, $CH_2$ and CH of PAM and PNaSS, $CH_2$ and $CH_3$ of PDMC, $-CH_2-NC_3$ of PDMC appear on the NMR spectrum of the polymer, which proves our original assumption that AM monomers disperse in the aqueous phase can penetrate DMC-NaSS micelles to copolymerize with hydrophobic styrene or with the surrounding hydrophilic amide groups (Scheme 1d), promoting hydrogel formation.

## Characterization of the hydrogel structure

**Transmission Electron Microscope (TEM).** In hydrogel polymerization, the water-soluble monomer AM is first dissolved in the aqueous phase while the amphiphilic DMC-NaSS self-assembles into the nano-micelles in solution. During polymerization, the PAM chain can cross multiple nano-micelles to form a dynamic crosslinked structure in which multiple hydrophobic groups are embedded in the hydrophilic polymer chain (Figure 1d). In order to verify the above assembly and polymerization process, DMC-NaSS solution and DMC-NaSS hydrogels with different HAc concentrations were observed by TEM, All samples were negatively stained with 2% phosphotungstic acid, and the liquid samples were firstly dispersed by ultrasound for 15min before observation. For gel samples, we used the (Leica EMFC7) Leica frozen ultra-thin microtome to cut the DMC-NaSS gel into nano-sheets with a thickness of 50 nanometers. That is, the epoxy resin was used to embed the sample; the sample was solidified, modified, frozen with nitrogen, and sliced. Then the nanofilm was placed on the carbon support film copper net. Finally, (JEM-2100) transmission electron microscope was used to characterize its structure. As can be seen from the Fig. S4a, the micelles in the DMC-NaSS solution without HAc have large particle size and uneven particle size distribution. In addition, there are many broken micelles in the field of view, indicating that without the strengthening effect of HAc on DMC-NaSS, the stability of DMC-NaSS micelles is very poor. However, the addition of HAc can

significantly reduce the particle size of micelles, and make their distribution more uniform and stability higher (Figure S6b-c). Figure S4d and Figure S6e are TEM images of DMC-NaSS hydrogel cross sections with and without 0.22mM acetic acid respectively. Compared with the amorphous morphology of the hydrogel surface in Figure S6d, a large number of DMC-NaSS micelles with regular morphology existed on the hydrogel surface in Figure S6e, indicating that without dipole interaction between acetic acid and quaternary ammonium, the DMC-NaSS micelles will be destroyed in the polymerization process.

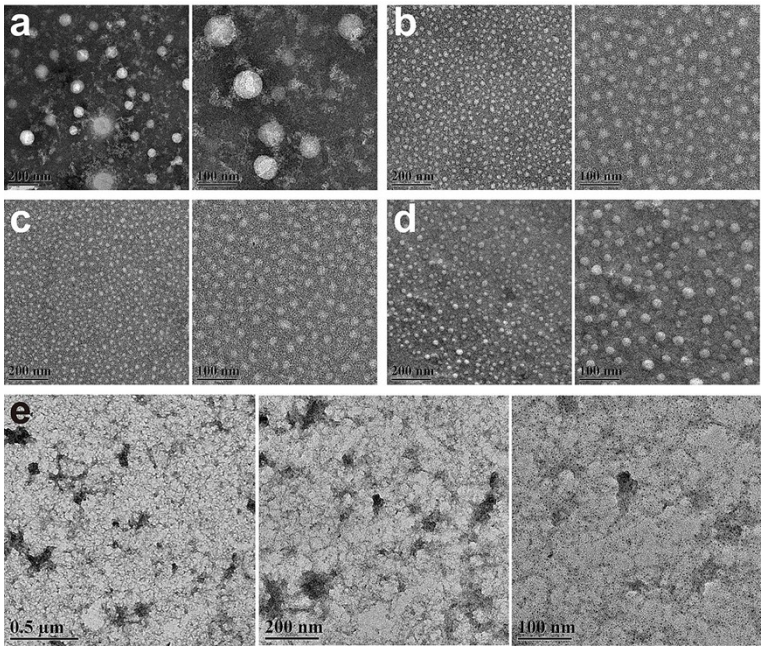


**Figure S6.** TEM morphology of DMC-NaSS micelles in the solution, (a) without HAc and (b-c) with HAc ((b) for 0.22mM and (c) for 0.44mM) at different magnification . TEM morphology of DMC-NaSS micelles in the hydrogel, (d) with HAc and (e) without HAc.

**Scanning Electron Microscope (SEM).** In order to verify the hydrogel's structure, the hydrogel was first freeze-dried overnight to remove excess moisture while its original three-dimensional network structure was maintained; the scanning electron microscope was used to observe the gel's microscopic morphology. Figure S7 shows that the target

hydrogel has a smaller, more regular and thicker pore structure than pure PAM hydrogel, which demonstrates that DMC-NaSS can promote the association of polymer chains. The formed nano-micelles make the internal spatial structure more dense and compact. As a result, the wall between the pores is thicker and stronger. When the monomers polymerize, the DMC-NaSS are linked by HAc, and so enhances the stability in the morphology of nano-micelles. Therefore, the pore structure of the gel is not easily destroyed and its overall mechanical properties are enhanced.

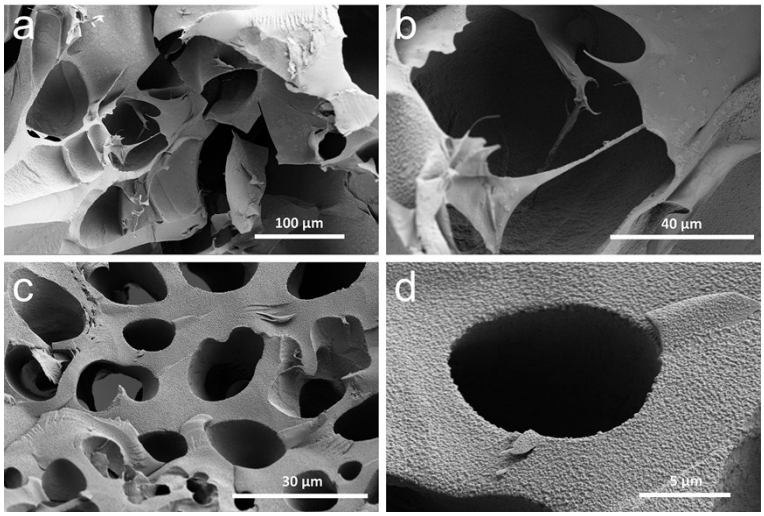


**Figure S7.** SEM morphology of dried PAM (c-d) and DMC-NaSS hydrogels (a-b).

## Characterization of the structure of water-equilibrated hydrogels.

In order to verify that the DMC-NaSS nanoparticles in the gel existed as micelles instead of DMC-NaSS crystals, DMC-NASS hydrogels with and without HAc were subjected to transmission electron microscopy test, respectively. the as-prepared hydrogels were immersed in a plenty of deionized water for 3 d with changing the water per every 12 hours to wash away part of the salt ions within the hydrogels. It can be seen from Figure S8(a-c) that the TEM image of the gel after water-equilibrated is similar to the gel sample before treatment. DMC-NaSS nanoparticles were not destroyed by a large amount of water, indicating that it is not a crystalline structure formed by a large number of DMC-NaSS dimers, but a micelle structure. Similarly, the presence of DMC-NaSS micelles can be seen in the TEM images of HAc-free hydrogel, indicating that the image in Figure S6a is micellar structure rather than crystal structure Figure S8d.

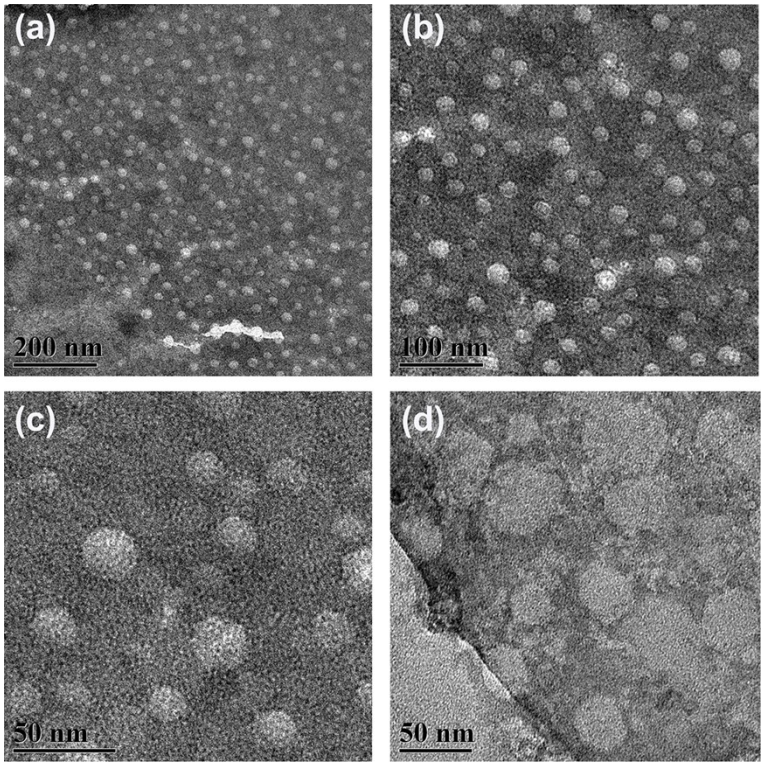


**Figure S8**. TEM morphology of micelles in water-equilibrated DMC-NaSS hydrogel (a-c), and water-equilibrated HAc-free DMC-NaSS hydrogel (d).

## Hydrogel stability in solutions with different pH values and electrolyte concentrations

The hydrogel was placed in aqueous solutions, varying in pH values, for 24 h, then their swelling ratios $Q_v$ ($=V_{swelling}/V_{original}$) and modulus of the hydrogel were measured (Figure S9a). As shown in Figure S9c the hydrogel is resistant to strongly acidic and alkali conditions, displaying stable volume and mechanical properties in different pH environments. Throughout the full pH range (pH=0-14), the volume exchange rate of the hydrogel is <130%, with its modulus remaining stable under weak acidic and strong alkali conditions, indicating that the hydrogel has the potential to resist complex external environments. Furthermore, the hydrogel samples were also immersed in aqueous solutions with different NaCl concentrations for 24 h (Figure S9b), after which the swelling ratios and modulus were measured. Figure S9d shows that the high electrolyte concentration has a great impact on the hydrogel's mechanical properties, with the gel's modulus exhibiting a significantly segmented phenomenon to NaCl concentration change. When the concentration increases from 0.5 to 1 M, a sharp decrease in the gel's modulus is observed; as the concentration further increases from 1 to 2.5M, the modulus gradually decreases. This is due to the electrolyte molecules destroying the hydrogel's electrostatic interactions.[5] Therefore, small molecular ions with positive and negative charges will accumulate on the outside of the electrolyte molecules poly-cations and anions forming a dynamic induction layer, which can weaken the polarities of these two ions and reduce the electrostatic interaction.

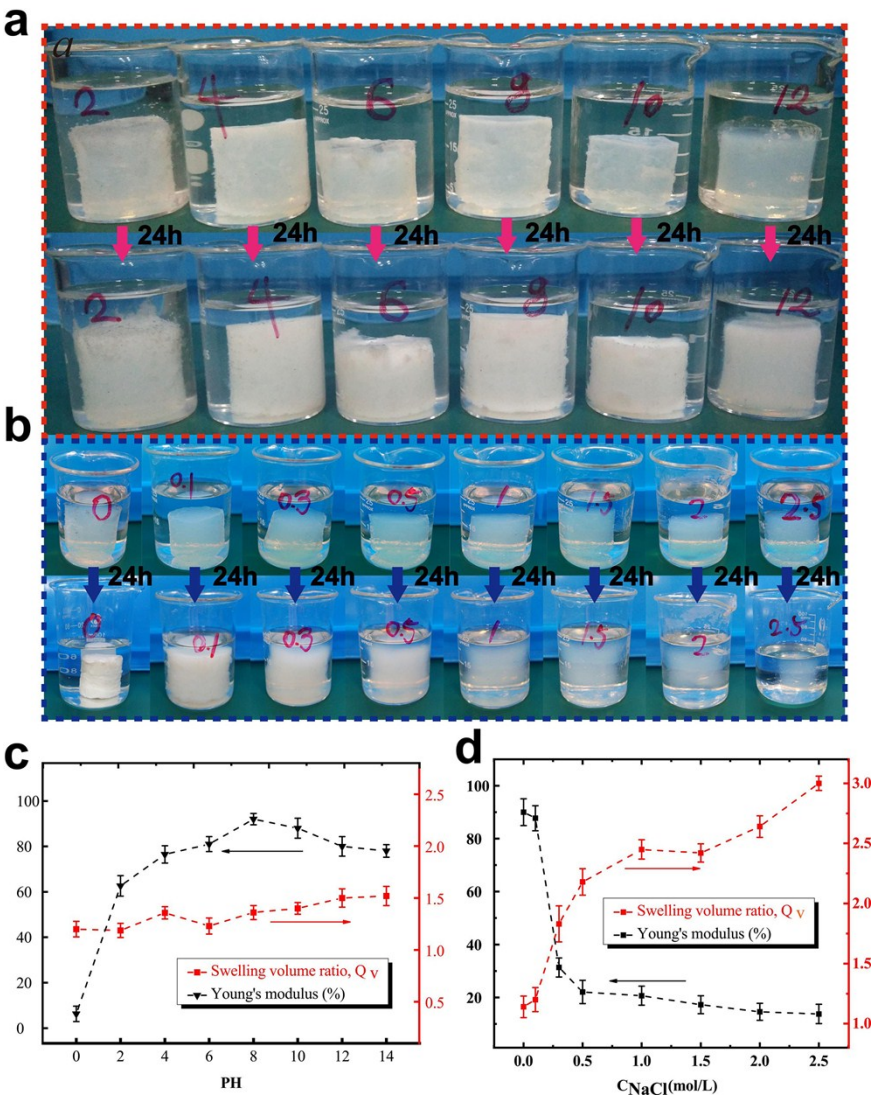


**Figure S9.** (a) Changes in the appearance of the gel after soaking in different pH solutions for 24 hours. (b) Changes in the appearance of the gel after soaking in different salt concentration solutions for 24 hours. Effect of pH and salt concentration on the volume ratio $Q_V$ and (the initial young's modulus of the DMC-NaSS hydrogel E) %. (c) pH effect, (d) salt concentration effect.

## Mechanical properties of hydrogel

**Tensile test of prepared hydrogel.** The tensile test of the gel was performed using an electronic universal tester (Instron, 5567, USA). The loading rate was 100 mm/min. The samples were 5 mm in height and 2 mm in diameter. The spacing between the labeled points on clamp was 2 mm. The nominal stress (σ) was calculated as:

$$\sigma = F / A$$

Where F denotes the tensile load of hydrogel and A denotes the original cross-sectional area.

The extension ratio (λ) is defined as:

$$\lambda = l / l_0$$

Where $l_0$ denotes the gel's original length and $l$ denotes the deformed length of the gel.

As shown in Figure S10, the gel has good recovery, reverting to its original length at once after break.

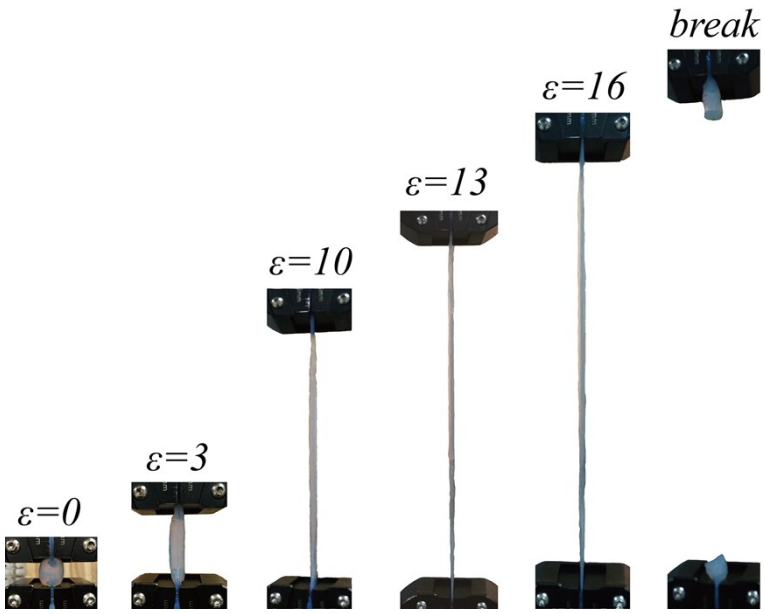


**Figure S10.** Pictures of a DMC-NaSS hydrogel at different strains, ε , when subjected to uniaxial tensile test.

**Successive loading-unloading compression tests of DMC-NaSS hydrogel.** The test was carried out on the electronic universal tester (Instron, 5567, USA), with a loading rate of 20 mm/min. Each cycle interval is 2min.

**Compression test of the prepared hydrogel.** The compression test of the hydrogel was carried out using the compression mode on the electronic universal tester (AI-700M), with a loading rate of 20 mm/min. Each sample was 1.5 cm in height and 2 cm in diameter. In order to prove that the hydrogel has superior compressive capacity, the maximum stress applied to the sample was 30 MPa. The stress-strain curves of the target hydrogel and pure PAM hydrogel are respectively shown in Figure 1f. Figure S11 shows images of the hydrogel and pure PAM hydrogel after unloading, where pure PAM hydrogel is completely crushed under 26 MPa of stress and the target hydrogel recovers to its initial state after unloading. Under the same loading conditions, the two kind of hydrogels with identical monomer concentration show different responses and

form a sharp contrast, which directly demonstrates that the target hydrogel's compressive resistance is superior to that of conventional homopolymeric hydrogel, and possesses the ability to carry excessively high loads.

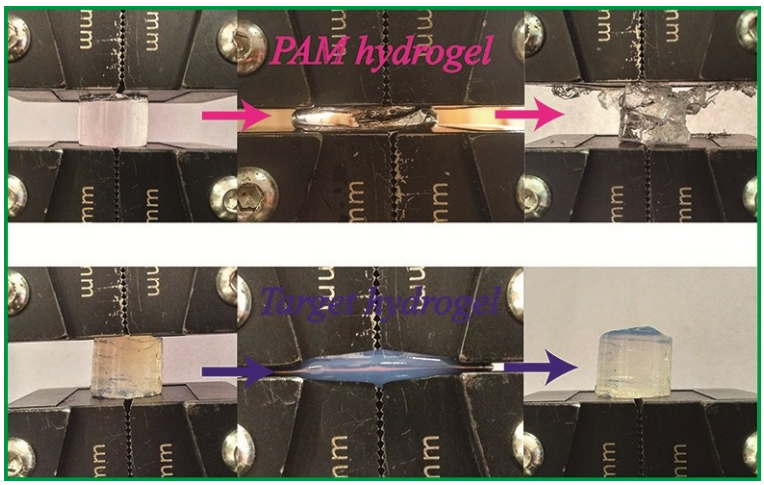


**Figure S11.** PAM and DMC-NaSS gel specimens with 2 cm in diameter and 1.5 cm in height before, during and after compressing.

**Determination of the fracture energy (Gc).** The fracture energy of the gel was performed on an electronic universal testing machine (Instron 5567) using the classic unilateral notch test. The crosshead speed was 2 mm/sec. Fix the sample between the fixtures with a gage length of $1_0$ = 10 mm (Figure S12a). The thickness and width of the samples were 5 mm and 30 mm, respectively. During the test, a pair of samples were pulled out: one sample was unnotched and the other was notched (Figure S12b). The unnotched specimen was pulled to obtain the stress-strain curve, whereas the notched specimen was used to determine the critical extension ratio ($\lambda_c$), at which cracks expanded. As for the notched specimen, a notch with the length of 5 mm was made in the middle of the specimens (Figure S12a). The fracture energy (Gc, $Jm^{-2}$) is calculated using the Equation (1) proposed by Greensmith for elastomers [8].

$$G_c = \frac{1}{B}\left[\frac{\partial(\Delta U)}{\partial a}\right] = 2\frac{\pi}{\sqrt{\lambda_c}} a w_0 \tag{8-1}$$

Where a is the length of the crack; $\lambda_c$ is the propagation rate of the crack in the single-edge notch test. In the current study, crack propagation is slow and it is difficult to record where the notch becomes a continuous crack. Therefore, the force is maximized during the pulling of the notched sample. $W_0$ is the strain energy density, which is obtained by integrating the stress and engineering strain of the unnotched samples, until $\lambda_c$ ($\lambda_c$=$\varepsilon_c$+1).

The calculation method of Gc is mature and has been widely used to test the breaking energy of the elastomer[8]. According to calculations, The fracture energy of the 1M DMC-NaSS hydrogel (1900 $Jm^{-2}$) is much higher than that of the pure PAM hydrogel (550 $Jm^{-2}$) and human cartilage (~1000 $Jm^{-2}$),[9] the breaking energy of the pure PAM hydrogel is 550 $J/m^2$, which is the same as the reported level. Previous research (250 J/m2)[9]. The consistency between our data and previous studies proves

that the calculation methods and data are reliable.

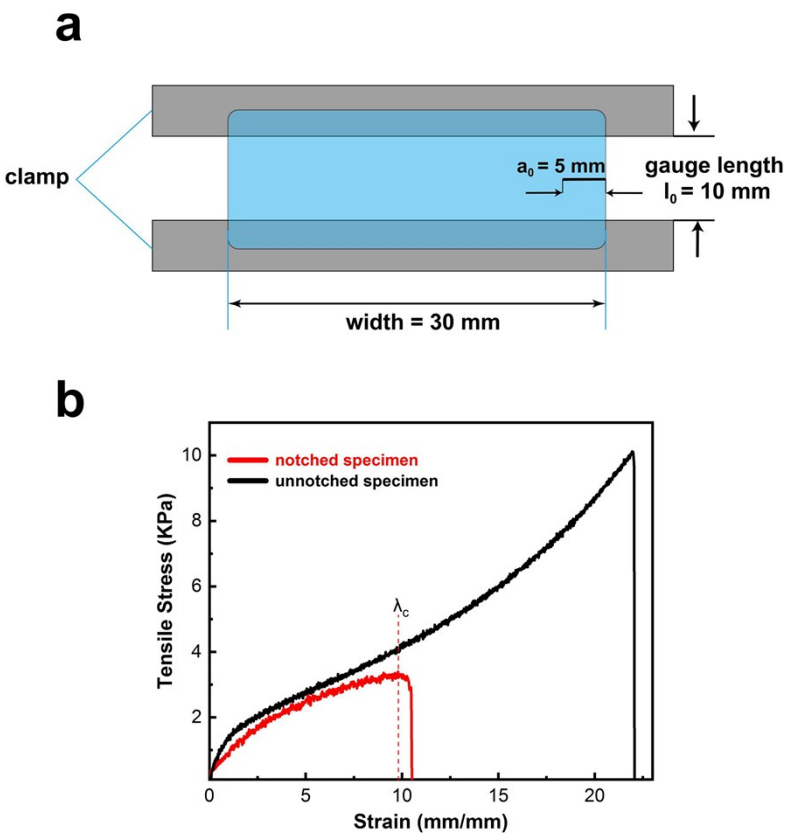


**Figure S12.** Single edge notch test to determine the fracture energy. (a) Geometry of notched specimen for single edge notch test. (b) Stress-strain curves of the unnotched (black) and notched (red) specimens.

## Analysis of the hydrogel's rheological behavior

**Experimental :** The rheological test[6] for the hydrogel was carried out on a rheometer with strain control (Anton Paar MCR-301) in order to characterize the dynamic rheological characteristics of PAM-PDMC-PNaSS hydrogel. The rheometer was equipped with two parallel plates with a diameter of 20 mm. The hydrogel was placed into the 0.5 mm spacing between plates. In order to prevent drying of the hydrogel, water was pasted around the hydrogel's external edge. Before the test, the strain amplitude scan was first performed (0.01-100%) to determine the linear viscoelastic region. Then the dynamic frequency scan was performed with the strain frequency ca. 1.0% (linear region) and angular velocity range of 0.01~10 Hz.

**Results :** Generally, the storage modulus represents the gel's strength while the loss tangent (the ratio between the loss modulus and storage modulus) represents its relative viscosity, which is beneficial to the rapid healing and performance recovery of the hydrogel after it is subjected to extreme force. As shown in Fig. S13, the storage modulus of DMC-NaSS hydrogels gradually increases with increasing concentration of DMC-NaSS, indicating that DMC-NaSS enhances the strength of the gel. However, in contrast to the storage modulus, the loss tangent of DMC-NaSS hydrogels decreases gradually with increasing concentration of DMC-NaSS, indicating that excessive DMC-NaSS concentration may decreases the self-healing ability of the DMC-NaSS hydrogel.

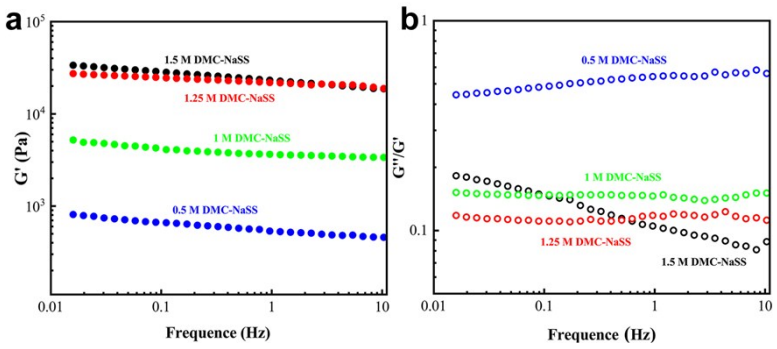


**Figure S13.** Viscoelasticity of DMC-NaSS hydrogels with different DMC-NaSS concentration. (a) Storage modulus (G') and (b) loss tangent (G''/G') of the hydrogels.

## Analysis of the hydrogel's self-healing capability

**Tensile-healing-tensile test.** Utilizing the tensile-healing-tensile test, the self-healing capability of the hydrogel was quantitatively analyzed (Figure 2c). First the samples with the same formulation were cut in two; these halves were then combined without any external force and additional conditions. The normal tensile tests were performed on the original sample and gel samples undergoing different healing periods. The tensile-healing-tensile test was conducted on the electronic universal tester (Instron, 5567, USA)

**Dynamic rheological test**

**Experimental**: The hydrogel's self-healing capability was verified using the dynamic rheological test.[7] First, 1000% strain amplitude sweep was applied to the hydrogel to rapidly reduce the storage modulus G' (Figure S14a, c). Then the strain amplitude sweep with low amplitude (0.01%) and low frequency (1 Hz) were applied to the hydrogel to complete the self-healing process (Figure S14b, d). Simultaneously, the gel samples's healing procedure was monitored.

**Results:** Figure S14b shows that after 100 s of self-healing, PAM-PDMC-PNaSS hydrogel shows almost full recovery to its original storage modulus (4230 Pa), while the modulus of pure PAM hydrogel is vastly different than its original value (34096.8 Pa) under the same conditions (Figure S14d). Experiments indicate that several reversible crosslinking characteristics make the hydrogel self-heal quickly after damage, including the electrostatic interaction between PDMC and PNaSS in the hydrogel gel, the hydrophobic interaction between DMC-NaSS and DMC-NaSS, etc.

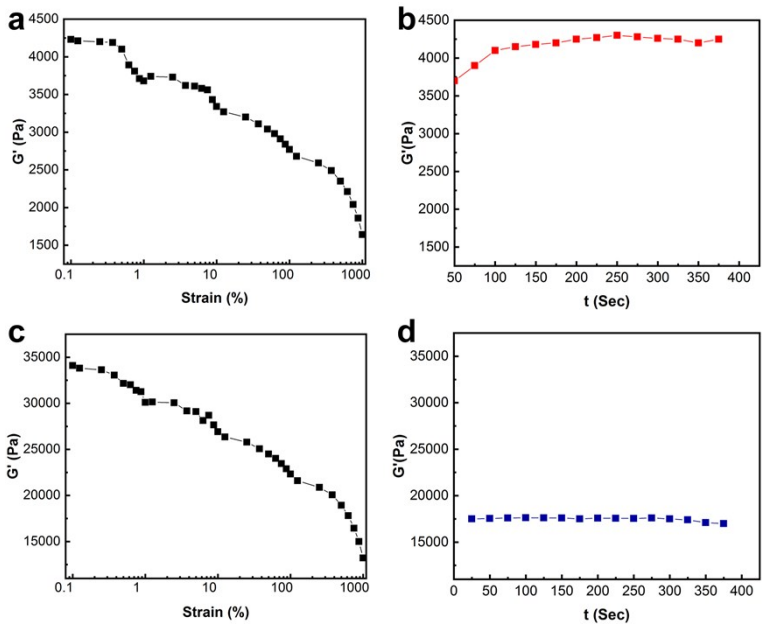


**Figure S14.** Dynamic rheological experiments illustrated the self-healing properties of (a-b) the DMC-NaSS hydrogel and (c-d) the pure PAM hydrogel.

## References


1. Liu, Y. L.; Ai, K. L.; Lu, L. H.; *CHEM REV.* **2014**, *114*, 5057-5115.
2. Jeon, I.; Cui, J. X.; Illeperuma, W. R. K.; Aizenberg, J.; Vlassak, J. J. *Adv. Mater.* **2016**, *28*, 4678-4683.
3. Hu, X. Z.; Liu, J. H.; He, Q. J.; Meng, Y.; Cao, L.; Sun, Y. P.; Chen, J. J.; Lu, F. S. *J. Name*. **2013**, *1*, 426-429
4. Basak, S.; Singh, I.; Kraatz, H-B. *CHEMISTRYSELECT.* **2017**, *2*, 451-457.
5. Kevin, J.; De, F.; Todd, H.; Emily, D. C. *Chem. Mater*. **2017**, *29*, 4609-4616.
6. Bani, H. C.; Stephen, J. B.; Renu, S.; Dominic, R.; Wonseok, H.; Robert, M. B.; Srinivasa, R. R. *Macromolecules.* **2014**, *47*, 4445-4451.
7. Han, L.; Yan, L.W.; Wang, K. F.; Fang, L. M.; Zhang, H. P.; Tang, Y. H.; Ding, Y. h.; Weng, L. T.; Xu, J. L.; Weng, J.; Liu, Y. J.; Ren, F. Z.; Lu, X. *NPG Asia Mater*. **2017**, *10*, 1038-1049.
8. Ducrot, E.; Chen, Y.; Bulters, M.; Sijbesma, R. P. & Creton, C. *Science.* **2014**, *344*, 186-189.

9. Sun, J. Y.; Zhao, X.; Illeperuma, W. R.; Chaudhuri, O.; Oh, K. H.; Mooney, D. J.; Vlassak, J. J. & Suo, Z. *Nature.* **2012**, *489*,133-136.